Design, manufacture, and testing of a magnetically shielded krypton Hall effect thruster

ESTORIL, PORTUGAL / 17-19 MARCH 2021

Thomas F. Munro-O'Brien[(1)] and Charles N. Ryan[(2)]
[(1) (2)] *University of Southampton, Highfield campus, Southampton, SO17 1BJ, United Kingdom*
Email: tfmo1e17@soton.ac.uk, c.n.ryan@soton.ac.uk

KEYWORDS

Electric propulsion, Hall effect thruster, Experimental, Alternative propellants, Low power, Magnetically shielded.

ABSTRACT

Typically, Hall Effect thrusters have been designed to operate in the kW regime, but due to their desirable thrust to power ratio and reliability they have recently undergone a significant amount of research to miniaturise and optimise for small satellites.

Within the Astronautics group at the University of Southampton, the design, manufacture, and testing of a 100 W miniature, annular, krypton Hall effect thruster with magnetic shielding was undertaken. This thruster, designated MaSHEKT-100, was tested with krypton propellant over anode powers of 30 W - 450 W, and anode voltages of 100 V - 600 V. The highest performance was measured at 540 V with 5.43 mN of thrust and 10.8 % anode efficiency. The designing of this thruster followed two main scaling methods comparing and combining the results of both with target parameters of 100 W power and 300 V anode voltage [1, 2].

The design method was also partially extended to compare designs for various alternative propellants. Xenon, krypton, and magnesium are investigated as these have been previously identified as viable alternatives [3]. The resulting thruster was sized with a mean channel diameter, channel length and channel width of, $d = 30$ mm, $L = 32$ mm, $h = 5$ mm, respectively.

1. INTRODUCTION

For the last half a century, space propulsion has utilised Hall effect thrusters (HET) in the kilowatt regime to great success. In recent years, the power available to large satellites has continued to grow [4], although in the last decade there has been a fast growing demand for electric propulsion from micro and nano class satellites. These smaller scale satellites lack the large power sources afforded to larger missions in the past [5], with the power available to the electric propulsion system limited to hundreds of Watts. For Hall effect thrusters to be applied to these power regimes, they need to be scaled down in terms of input power, as well as physically.

The design, manufacture, and testing of a low powered Hall effect thruster was undertaken by following published scaling methods. The thruster was designated the MaSHEKT-100, the Magnetically Shielded Hall Effect Krypton Thruster designed for 100 W anode power. The MaSHEKT-100 was subsequently tested with krypton within the large vacuum chamber facilities at the University of Southampton over a power range of 30 W - 450 W, and a range of anode mass flow rates of 5-11.5 standard cubic centimetres per minute (sccm) of krypton. Over this range the thruster exhibited thrusts of 4-5 mN at specific impulses up to 1200 s and anode efficiencies up to 10.8 %.

2. HALL EFFECT THRUSTER DESIGN

2.1 Alternative propellant considerations

During the design of the thruster, alternative propellants were considered by taking into account the effect on performance of the differing atomic mass, ionisation energies, and the cross-sectional areas of impact ionisation. Although, to understand ionisation for the effective consideration of alternative propellants, a way of quantifying ionisation is needed. One such method is the Melikov–Morozov criterion, as this has a strong impact on effective ionisation within a HET. This criterion states that free path of ionisation must be significantly less than the chan-

nel length [1, 2],

$$\lambda_i << L \qquad \text{Eq.1}$$

where λ_i is the ionisation free path, and L is the channel length from anode to channel exit. Given ν_i is the ionisation frequency resulting from electron-neutral impacts. This can be expressed as,

$$\nu_i = n_n \langle \sigma_i v_e \rangle \qquad \text{Eq.2}$$

where n_n is the neutral number density, σ_i is the cross-sectional area for impact ionisation of the propellant, and v_e is the electron velocity. The Melikov-Morozov criterion can therefore be described as,

$$\lambda_i = \frac{v_n}{n_n \langle \sigma_i v_e \rangle} << L \qquad \text{Eq.3}$$

where $\langle \sigma_i v_e \rangle$ is the reaction rate coefficient, normally on the order of $0.5 - 4(\times 10^{-13})$, and v_n is the assumed thermal velocity of the propellant. It is important to note that $\langle \sigma_i v_e \rangle \neq \sigma_i v_e$ as the electron energy distribution will have additional contributions to ionising collisions that the mean electron velocity cannot capture.

Changing the propellant has several effects on Eq.3. A lighter element would have a greater v_n for the same anode temperature, a different mass flow rate to achieve the same n_n, as well as different electron impact ionisation cross-sectional area, when compared to xenon.

To investigate the effects that alternative propellants have on ionisation, a range of measurements of cross-sectional area of ionisation were used. The values used and compared are from both experimental and numerical results for various elements, available from independent studies.

The reaction rate coefficient, $\langle \sigma_i v_e \rangle$, is the resultant product of probabilistic velocity of the electrons at a particular electron temperature, and the cross-sectional area of inelastic interaction for the neutral atoms in the plasma. This estimate of ionization rate is calculated by integrating a Maxwellian-Boltzmann distribution of the microscopic (individual) electron velocity of thermal origin, defined as w [6]. The 3-dimensional velocity w described independent of the directional velocity is,

$$g(w) = \sqrt{\frac{2}{\pi}} \left(\frac{m_e}{k_B T} \right)^{3/2} w^2 exp\left[-\frac{m_e w^2}{2 k_B T} \right] \qquad \text{Eq.4}$$

where T is the electron temperature in Kelvin, m_e is the electron mass, and k_B is the Boltzmann constant. This integral can be expressed as a function of electron temperature [7],

$$\langle \sigma_i v_e \rangle (T_{eV}) = \int_0^{+\infty} w \sigma_i (T_{eV}) g(w) dw \qquad \text{Eq.5}$$

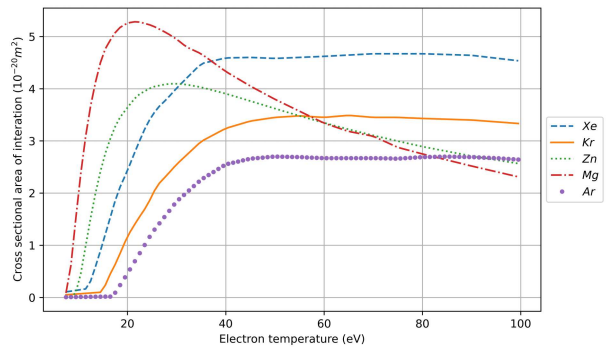

Figure 1: A comparison of the cross-sectional area of impact ionisation of various potential propellants under consideration. Cross-sectional area data is sourced from the following: xenon and krypton - [8], zinc and magnesium - [9], and argon - [10]. Ref. [8, 10] data is from experiments, and Ref. [9] is from computational simulations.

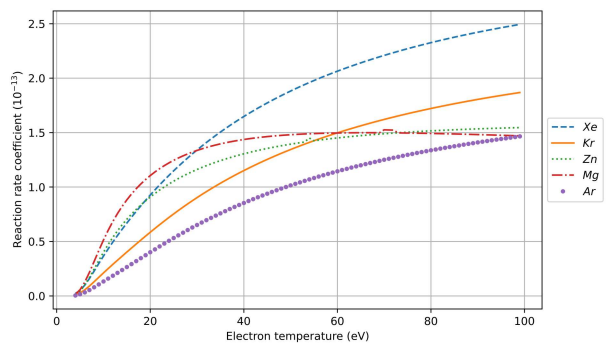

Figure 2: Shows the calculated reaction rate coefficient against bulk electron temperature for the propellants considered in Fig. 1 by using a computational result of Eq.5.

Eq.5 was numerically solved using the Numpy Python 3.2 library. Where σ_i is a function of electron temperature in electron volts, and $g(w_n)$ is the function as described in Eq.4. The results of this calculation for several elements can be seen in Fig. 2.

2.2 Scaling methodology

The scaling methodologies used were those of Dannenmeyer and Mazouffre [1] and Lee et al. [2]. Both share similarities, with both methods derived from correlations present in databases of proven thrusters, in conjunction with simplified plasma and performance equations. Dannenmeyer [1] uses a database of 33 thrusters ranging in power of 10 W

- 50 kW, whilst Lee [2] used 17 exclusively sub-kW thrusters with only slight variations on the scaling equations used. Both methods are based around setting up a group of equations that allow a complete thruster channel geometry to be obtained from an input anode power and voltage.

These scaling methods require several assumptions and stipulations. Firstly, the anode mass flow rate is chosen to meet an optimal number density. From literature, this has been seen to be $n_n \approx 1.2 \times 10^{19}\ m^{-3}$, with the electron number density was also found to be $\approx 0.1 \times n_n = 1.2 \times 10^{18}\ m^{-3}$. This ensures a sufficient rate of ionisation and optimal thermal effects, as found by [11]. The electron temperature is also a very important parameter to characterise the plasma and its behaviour. An estimation of the bulk electron temperature is [1],

$$T_{eV} \approx 0.2 U_d \qquad \text{Eq.6}$$

where U_d is the anode discharge voltage. It is also assumed that the neutral propellant is released at a temperature of 800 K, although in literature this value has been varied between $800 - 1300$ K for the same calculation [1, 7, 12]. For the calculation within this paper 800 K was used, although this range has a non-negligible effect on the ionisation free path and highlights another potential issue with this method of scaling. For example, xenon at 800 K and 1300 K has a neutral velocity of 360 m/s and 460 m/s, respectively.

2.2.1 Scaling equations

The equations that form the scaling methods will not be fully derived here but the initial equations and the final scaling group will be shown.

Firstly, the Melikov–Morozov criterion, seen in Eq.1, is used to ensure sufficient ionisation. The equations try to preserve the plasma's physical behaviour over a range of power, so the relations of electron confinement need to be preserved. This is achieved by the following criterion,

$$r_{Le} << L \qquad \text{Eq.7}$$

where r_{Le} is the electron Larmor radius, the radius of the electron circular motion within the magnetic field. Ensuring this radius is much smaller than the channel length, the electrons will not be impacting the walls. The definition of the electron Larmor radius is,

$$r_{Le} = \frac{m_e v_e(Te)}{eB} \qquad \text{Eq.8}$$

where e is the elementary charge and B is the field strength. Secondly, for effective electron confinement, the electron gyro-period needs to be significantly shorter than collision period. Such that,

$$\frac{\tau_{en}}{\tau_{ce}} = \frac{\omega_{ce}}{\nu_{en}} >> 1 \qquad \text{Eq.9}$$

where $\tau_{en} = 1/\nu_{en}$, τ_{ce} is the electron gyro-period and ω_{ce} is the electron gyrofrequency. The fulfilment of these two criteria is required for all HETs, as the trapping of a sufficient number of electrons is required for the large potentials that accelerate the ions.

The relationship between the scaling and mass flow rate is strongly tied to the assumption of $n_n = 1.2 \times 10^{19}\ m^{-3}$ and described with,

$$\dot{m}_n = n_n \times m_n \times v_n \times A_c \qquad \text{Eq.10}$$

where m_n is the neutral atomic mass and A_c is the cross-sectional area of the channel. From this it can be seen that,

$$n_n \propto \frac{\dot{m}_n}{hd} \qquad \text{Eq.11}$$

where h, and d are the channel width, and mean channel diameter, respectively. After this several other relations are formed with performance values that can be easily measured and are available from the databases of thruster performance.

The scaling group of equations as derived by Dannenmeyer [1] are,

$$T_1 = C_{T_1} \dot{m}_n \sqrt{U_d} \qquad \text{Eq.12}$$

$$T_2 = C_{T_2} d^2 \sqrt{U_d} \qquad \text{Eq.13}$$

$$I_{sp} = C_{I_{sp}} \sqrt{U_d} \qquad \text{Eq.14}$$

$$I_d = C_I d^2 \qquad \text{Eq.15}$$

$$P = C_P d^2 \sqrt{U_d} \qquad \text{Eq.16}$$

$$h = C_{hd} d \qquad \text{Eq.17}$$

and those derived by Lee [2] are as follows,

$$T = C_T \dot{m}_n \sqrt{U_d} \qquad \text{Eq.18}$$

$$P_d = C_p U_d d^2 \qquad \text{Eq.19}$$

$$\dot{m}_n = C_{\dot{m}} hd \qquad \text{Eq.20}$$

$$h = C_{hd} d \qquad \text{Eq.21}$$

where C_{T_1}, etc... are all coefficients of proportionality. It is noteworthy to mention that magnetic field

Scaling coefficient	value	units
Lee & et al. [2]		
C_T	892.7	$ms^{-1}\sqrt{V}^{-1}$
C_P	633	$kgs^{-2}V^{-1}$
$C_{\dot{m}}$	0.003	$kgm^{-2}s^{-1}$
C_{hd}	0.242	-
Dannenmeyer & Mazouffre [1]		
C_{T_1}	1077.3	$ms^{-1}\sqrt{V}^{-1}$
C_{T_2}	0.924	$kgm^{-1}s^{-2}\sqrt{V}^{-1}$
$C_{I_{sp}}$	109.835	$s\sqrt{V}^{-1}$
C_P	11928	$kgs^{-2}\sqrt{V}^{-1}$
C_{hd}	0.242	-
Hybrid		
C_{T_1}	854.1	$ms^{-1}\sqrt{V}^{-1}$
C_{T_2}	0.7153	$kgm^{-1}s^{-2}\sqrt{V}^{-1}$
$C_{I_{sp}}$	86.3	$s\sqrt{V}^{-1}$
C_P	11711	$kgs^{-2}\sqrt{V}^{-1}$
C_{hd}	0.256	-

Table 1: A comparison between the scaling coefficients for both [2] and [1]. The Hybrid section was computed using the method as constructed by Dannenmeyer and Mazouffre [1] with the database from Lee et al.[2]

strength is not directly related to the geometry for either of these scaling methods, with it assumed to be ≈ 200 G regardless of the discharge power [1, 2]. Although, should be considered post scaling and selected such that there is sufficient electron confinement, and the ions are not significantly magnetized. It is stated that $B \propto 1/hd$, suggesting that low powered, small HETs would require large field strengths [1]. The exclusion of magnetic field strength in scaling equations directly could limit this methods ability to appropriately scale a sub-kW HET.

2.2.2 Scaling coefficients

The scaling coefficients that relate to Eq.12 - Eq.21 are shown in Tab. 1. The Coefficients for a hybrid method are also shown, where the equations from [1] are used in conjunction with the database presented within [2].

2.2.3 Scaling results

It is important to understand that both methods used rely upon databases of existing thrusters, with the implications of using previously developed thrusters for the scaling laws. For example, all the database thrusters operated exclusively with xenon as a propellant. As a result, the ability to scale directly for

Output	Dannenmayer [1]	Lee [2]	Hybrid
d, mm	22.0	22.95	22.2
h, mm	5.32	5.5	5.68
F, mN	7.75	5.91	6.107
$\dot{m}_a$, mg/s	0.415	0.38	0.412
$\dot{m}_a$, sccm$_{Kr}$	6.7	6.1	6.6

Table 2: Outputted values for geometry of a HET with anode power of 100 W, discharge voltage of 300 V, and magnetic field strength of 200 G. This table compares the results from the [1], the [2] and a hybrid between the two.

thrusters using alternative propellants such as krypton or magnesium is not feasible. Moreover, the fact that field topology effects are omitted in scaling introduces numerous issues. Firstly, it limits the ability to physically design a magnetic circuit for the outputted geometry. Secondly, the overall effect of the topology, for example with a magnetic field designed to apply shielding, there is normally a pronounced gap between the plasma volume and the channel walls. This can be viewed as having an impact on the effective channel width and length. These clarifications do not remove the usefulness of these methods but do highlight the limitations for scaling to low powers, alternative propellants, and novel field topologies.

The scaling has succeeded in producing a reasonable sizing for a small HET of this power scale, although there are some irregularities with regards to how valid this approach is for low power HETs. For example, in both methods the channel width is calculated via the C_{hd} scaling coefficient, under the assumption that there is a strong relationship between the width and diameter. Whilst there is a strong correlation at the kilowatt regime, the deviation for sub-kW Hall thrusters is significant. Within the database provided by [2], the C_{hd} for each thruster is computed and compared. This shows, $\bar{C_{hd}} = 0.257$ and that $\sigma(C_{hd}) = 0.041$. This is a non-negligible deviation, suggesting that after scaling the h/d ratio can be subjected to more variation without losing the key plasma formation mechanisms. For example, the SPT-100 has a mean channel diameter of 85 mm and a channel width of 15 mm, for the same mean channel diameter this method suggests a channel width of 25.3 mm and 18.4 mm for one standard deviation plus and minus from the mean, respectively.

2.2.4 Selected geometry

The final design chosen for the MaSHEKT-100 did deviate from the suggested values produced by the

	Value
d, mm	30.0
h, mm	5.0
L, mm	32.4

Table 3: A table for the selected geometry for the MaSHEKT-100.

scaling method. This was primarily due to the intended inclusion of MS field topology. As a result, the magnetic circuit was more complex than could be easily implemented within the produced designs.

It is possible to compare the thruster's theoretical performance for various alternative propellants with the work completed in section 2.1. Firstly, thrust for an electric propulsion system can be expressed as,

$$T = v_{ex}\dot{m}_i \qquad \text{Eq.22}$$

where v_{ex} is the exit velocity, and $\dot{m}_i$ is the mass flow rate of ejected ions. Although this is an ideal equation, assuming that all ions are accelerated perfectly axially, and that all motion of electrons can be neglected.

Secondly, specific impulse of a thruster can be expressed as,

$$I_{sp} = \frac{T}{g_0\dot{m}_n} \qquad \text{Eq.23}$$

where g_0 is the gravitational rate of acceleration and $\dot{m}_n$ is the mass flow rate of neutral propellant. Thirdly, the total efficiency for an electric propulsion system can be described as,

$$\eta_a = \frac{P_{jet}}{P_{in}} \qquad \text{Eq.24}$$

where η_a is the anode efficiency and P_{jet}, and P_{in} are the jet power, and anode power, respectively [13]. P_{jet} can be described as the kinetic energy of the ejected mass, such that,

$$P_{jet} = \frac{1}{2}\dot{m}_i {v_{ex}}^2 \qquad \text{Eq.25}$$

with Eq.22 and Eq.24, it can be seen that,

$$\eta_a = \frac{T^2}{2\dot{m}_i P_{in}} \qquad \text{Eq.26}$$

For HETs, the mass of ejected fuel can be assumed as the mass of the ions accelerated by the electric field, where $\dot{m}_i$ and v_i are described as,

$$\dot{m}_i = \frac{I_b m_i}{q} \qquad \text{Eq.27}$$

and,

$$v_i = \sqrt{\frac{2qU_d}{m_i}} \qquad \text{Eq.28}$$

Value	Kr	Xe	Mg
$Thrust$, mN	4.70	5.88	2.53
Isp, s	1655	1322	3073
λ_i, mm	3.54	1.95	4.95
$\dot{m}_n$, mg/s	0.354	0.443	0.191
$\langle\sigma_i v_e\rangle$, $\times 10^{-13}$	1.059	1.535	1.405
η_a, %	31.2	39.1	16.8

Table 4: A comparison of predicted performance of the MaSHEKT-100 with alternative propellants using Eq.3, Eq.4,Eq.10, Eq.26, Eq.30, & Eq.31. All comparisons were done at 100 W anode power and 300 V anode voltage. [1, 8, 9, 13]

where q is the average charge of the ions, assumed to be equal to the elementary charge. Such as, Eq.22 and Eq.23 can be expressed as,

$$T = \sqrt{\frac{2m_i}{e}} I_b \sqrt{U_d} \qquad \text{Eq.29}$$

and,

$$I_{sp} = \frac{1}{g_0}\sqrt{\frac{2eU_d}{m_n}} \qquad \text{Eq.30}$$

where I_b is the ion beam current, and m_i is the mass of single ion. For krypton, $\sqrt{2m_i/e} = 1.32 \times 10^{-3}$ [13]. The beam current can be roughly approximated as the anode current, I_d, with the addition of an ionisation efficiency coefficient, α_e. To include the effects of beam divergence on thrust the γ_d correction factor is also included, allowing the final thrust equation to be,

$$T = \gamma_d \alpha_e \sqrt{\frac{2m_i}{e}} I_d \sqrt{U_d} \qquad \text{Eq.31}$$

For an anode voltage of $U_d = 300\ V$, this gives $\alpha_e \approx 0.71$, and that the beam divergence is normally $\approx 30°$, as a result, $\gamma_d \approx 0.87$ [1, 13].

With Eq.22 - Eq.31, and the information in section 2.1 an estimate for performance can be formed for alternative propellants.

The results of these calculations can be seen in Tab.4.

2.3 Field design

2.3.1 Field strength

Although the primary scaling laws considered here do not include magnetic field within the scaling [1, 11], these studies have included ways of estimating the post scaling magnetic field strength required. The scaling laws in these studies concerned with magnetic field are;

$$B_1 = C_{B_1}\frac{\sqrt{U_d}}{L} \qquad \text{Eq.32}$$

and,

$$B_2 = C_{B_2} \frac{\dot{m}_n \sqrt{U_d}}{d^2} \qquad \text{Eq.33}$$

Using these, a coefficient of magnetic field strength can be deduced from a database of thrusters resulting in $B_1 = 0.0447$ T, and $B_2 = 0.0117$ T from Eq.32 and Eq.33 respectively. This relatively large range is most likely due these zero-dimensional scaling models not encompassing the field topologies. With this, a target field strength was chosen to be 200 G as it was between the range and is the almost universally selected field strength for thrusters with flight history [1, 2, 11, 14, 15].

2.3.2 Magnetic shielded topology

For estimates of and one-dimensional simulations of HET it is common to assume that the magnetic field profile along the mean diameter can be described as, [16, 17]

$$B(z) = B_{Max} exp\left[-K\left(\frac{z}{L} - 1\right)^2\right] \qquad \text{Eq.34}$$

Eq.34 is the ideal magnetic field distribution for an unshielded HET, where K is the field shape coefficient, for the SPT-100 $K = 16$, and z is the distance from the anode. Once $z > L$ the field intensity decreases linearly.

The ability for HET to be magnetically shielded is a relatively new consideration. The widely accepted first instance of MS occurring was in 2010 by de Grys et al. [18], where after a long duration test of 5,600 hours, the erosion of the channel walls in the BPT-4000 appeared to completely stop. It was then postulated that by carefully designing the magnetic field topology at the channel exit, a zero-erosion state could be reached quickly, effectively extending the lifetime of the thruster considerably.

The main feature of MS topology is the magnetic field lines are parallel to the wall to prevent the impinging of electrons and maintain a high wall potential. For the MaSHEKT-100 the magnetic circuit selection was chosen to give a large amount of control and tune-ability to the magnetic profile. For this reason, 3 separate electromagnets were chosen to control the field strength in the entirety of the channel, two smaller coils and a main outer coil.

To design the thruster and the magnetic field topology a finite element software was utilised. "Finite Element Method Magnetics" (FEMM) is a two-dimensional simulation software that allows the modelling of material and magnetic fields. This was used to design and iterate through different coil configurations, until a final design was chosen [19, 20].

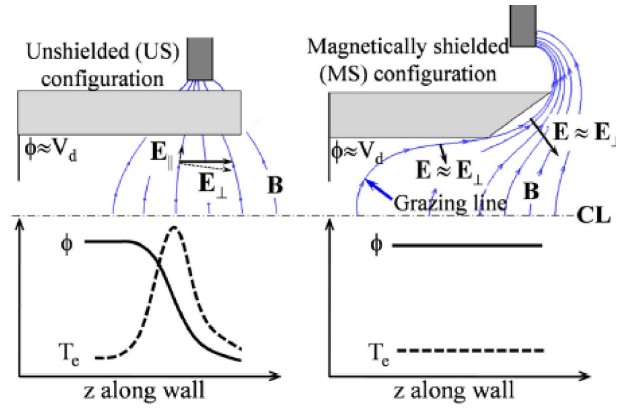

Figure 3: A comparison between the magnetic field lines and electron temperatures of an unshielded (US) and a magnetically shielded (MS) HET [19].

Coil	Current, A
Top coil	3.2
Trim coil	2.045
Outer coil	2.46

Table 5: The selected coil currents for adequate field strength and , a desirable field topology as suggested by FEMM simulations.

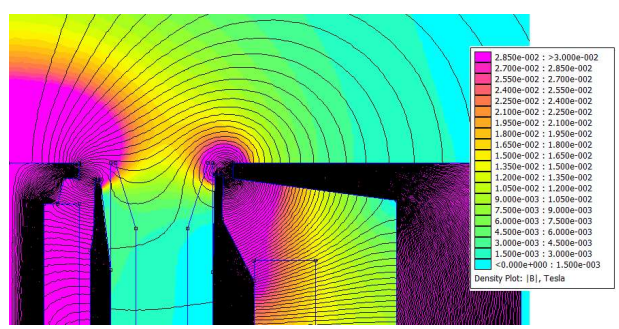

Figure 4: Magnetic field topology, designed and modelled in FEMM, using an axisystematic magnetic simulation.

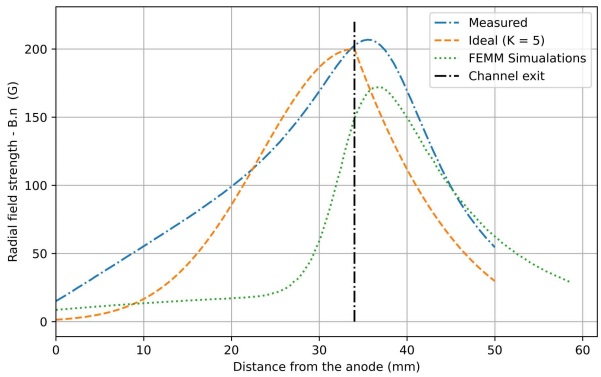

Figure 5: The radial field strength measured using a Hirst Magnetics GM07 Gauss Meter and a brushed motor translation stage. The coil currents used for this plot can be seen in Tab.5 and ideal case is described by Eq.34 [16, 17].

The results from the FEMM simulation can be seen in Fig. 4. Whilst this simulation suggests a MS field topology, as shown in Fig. 3, the field strength peaks at 240 G and is outside of the channel. In Fig. 5, the radial component of the field strength along the channel mean diameter line can be seen plotted against the actual readings of the manufactured thruster. It can be seen from this that the simulations significantly under compute the field strength and the profile. As a result, without further testing and measurements of the magnetic field, the validity of the magnetic shielding is unclear. This is planned to be addressed with a future long duration test and precise scanning of the channel.

The FEMM simulation assumed that the main body material was 1010 steel, in reality this was manufactured from a low-cost mild steel, this has appeared to have saturated much faster. This is a possible explanation for the stronger than expected magnetic field along the channel up to the exit.

As can be seen in Fig. 5 and 6, the peak field strength occurs beyond the channel exit. Although this is characteristic of magnetically shielded designs, it in of itself does not suggest that the final topology was shielded, but merely in-line with what would be expected of a shielded topology.

3. TESTING

3.1 Vacuum chamber

The main vacuum chamber consists of a 2 m diameter, 4 m long steel cylinder. The combination of vacuum, turbo, and cryogenic pumps results in the vacuum chamber achieving 7×10^{-8} millibar with no

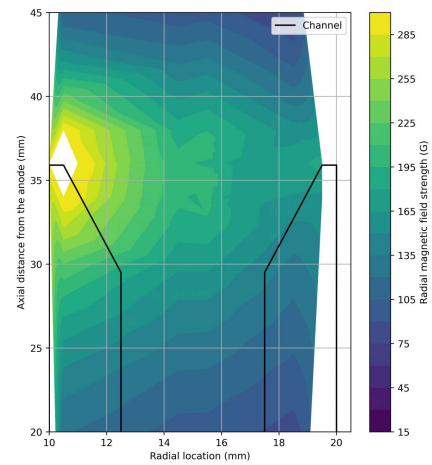

Figure 6: The radial field strength measured using a Hirst Magnetics GM07 Gauss Meter and a brushed motor translation stage. The coil currents used can be seen in Tab.5.

Figure 7: The MaSHEKT-100 operating within the large vacuum chamber at approximately 280 W with 6.0 sccm of krypton.

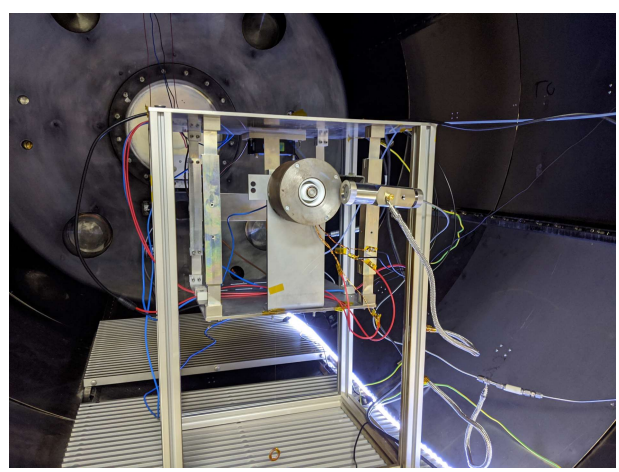

Figure 8: The MaSHEKT-100 mounted on the pendulum thrust stand in the large vacuum chamber at the University of Southampton before testing.

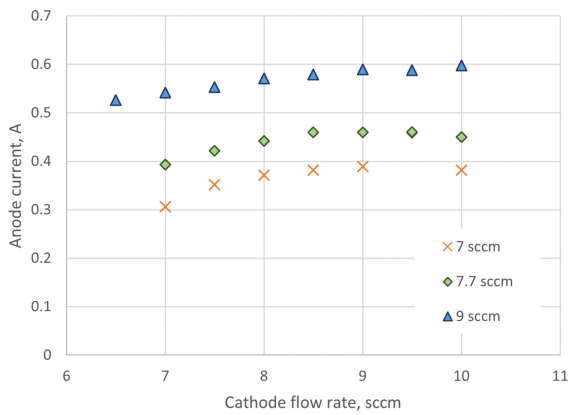

Figure 9: The effect on anode current as cathode flow rate is varied for three separate anode mass flow rates, all tests were conducted in a voltage limited state, with an anode voltage of 220 V.

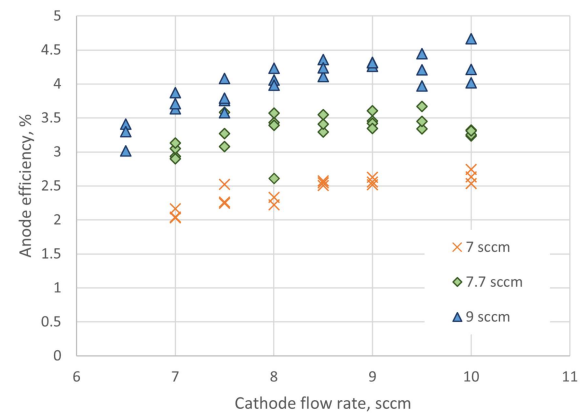

Figure 10: The effect on anode efficiency as cathode flow rate is varied for three separate anode mass flow rates, all tests were conducted in a voltage limited state, with an anode voltage of 220 V.

gas flow rate into the vacuum chamber, and of the order of $10^{-6} - 10^{-5}$ millibar when a flow rate of 1 – 10 sccm of krypton is fed into the vacuum chamber. The inside of the vacuum chamber can be seen in figure 8.

3.1.1 Cathode

The cathode used for the entirety of the testing was a "Model 5000 Hollow cathode electron source" from Iontech, a cathode designed to provide 0-20 amps to gridded and gridless ion sources. The cathode uses a tungsten filament for electron emission, and can be seen in Fig. 8 on the right-hand side of the thruster.

This cathode is not a space grade cathode and as a result it requires flow rates on the order of 10s of sccm, this is significantly higher than a normal space grade cathode. As a result, the total efficiencies have not been included as the high cathode flow rates cause these to be significantly reduced.

The anode and cathode were both run, for these tests, on krypton. As a result of the high flow rates the cathode requires, some unionised gas from the cathode could be entering the thruster causing additional thrust to be produced, this does bring into question the validity of the results of thruster performance. This has been investigated by measuring the performance of the thruster as the cathode flow was varied. The result of these tests can be seen in Fig. 9 and 10.

For the test data presented within this paper, the thruster was operated at using 8 sccm of krypton as the cathode flow, unless stated otherwise. This does have an influence on the performance although given context that Fig. 9 and 10 provides, this data is considered valid.

3.1.2 Thrust stand

The thrust stand used for all the testing, as seen in Fig. 8, was designed for testing for a cylindrical Hall thruster used by the University of Southampton for Undergraduate and Postgraduate laboratories [3]. The thrust stand uses a simple "Micro-epsilon 1700" laser triangulation sensor to measure displacement whilst under load. This was calibrated by using a brushed motor linear displacement stage to displace a known mass hung from the stand to apply a known force. The thrust stand was calibrated multiple times throughout the testing of the thruster. The calibration factor determined after the most recent calibration of the thrust was 295.12 ± 35.20 mN/mm. The error in this calibration is significant, at almost a 12 % range.. As a result, the thrust stand will hopefully be improved before future testing.

3.2 Testing methodology

For the vast majority of testing performed, the thruster was run in a voltage limited state. This was due in part to the two power supplies used were limited to 1 and 2 amps, respectively. So, to achieve desired power of several hundred Watts, it was necessary to operate at several hundred volts, with a sub-ampere discharge current.

The thruster would be powered on after a successful ignition of the cathode, little care was taken

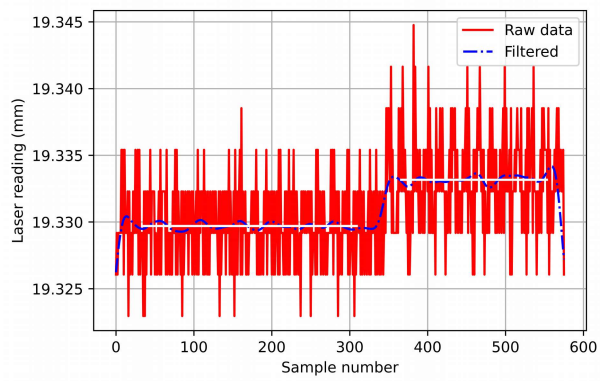

Figure 11: An example of the raw and filtered data from the thrust stand. The white lines indicate the mean values of the filtered data before and after thruster deactivation and the difference in these displacements were used to compute the thrust.

to ensure the thruster was up to a consistent temperature before data was recorded. As a result, all data points were recorded thrice at different times after ignition, such it was thought that any thermal variation would average out. Nothing was seen during these testing that could suggest a significant variation of performance with overall temperature.

4. RESULTS

4.1 Thruster performance

The equations used to evaluate the thruster are,

$$F = s_{dis} * C \qquad \text{Eq.35}$$

where s_{dis} is the measured displacement from the thrust stand and C is the calibration value. For much of the testing the calibration value used was 0.295 N/mm. An example of the raw and filtered thruster measurement can be seen in Fig. 11.

With the measured thrust and the known anode voltage, current, and mass flow rate, all performance values can be calculated. The specific impulse can be calculated using Eq.23 and Eq.35, where $\dot{m}_n$ is equal to the anode mass flow rate supplied. The Anode efficiency can also be calculated by using,

$$\eta_{anode} = \frac{F^2}{2P_{anode}\dot{m}_{anode}} \qquad \text{Eq.36}$$

where η_{anode}, P_{anode}, and $\dot{m}_{anode}$ are the anode efficiency, power, and mass flow rate, respectively [13].

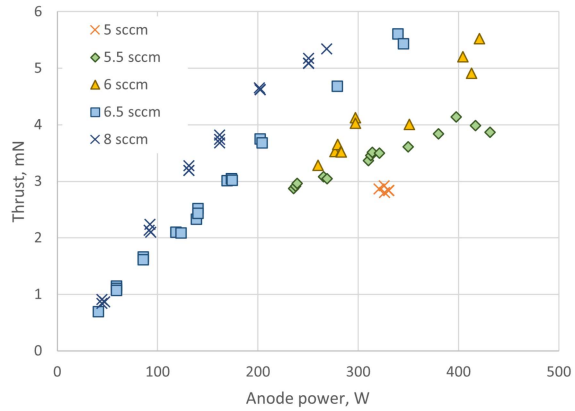

Figure 12: Effect of power on thrust for various anode mass flow rates, all tests were operated in a voltage limited state.

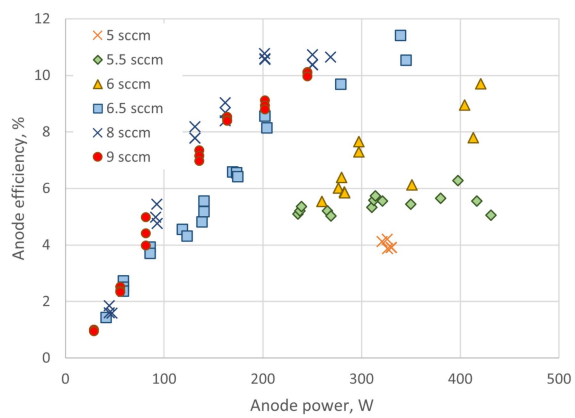

Figure 13: Effect of power on anode efficiency for various anode mass flow rates, all tests were operated in a voltage limited state.

4.1.1 Mass flow rate

Here the data produced by the thruster has been grouped by the anode mass flow rates. The thruster operated well at flow rates above 5 sccm of krypton, but had difficulties operating at lower flows, requiring the flow to be increased to ignite the thruster and subsequently lowered to the desired flow.

The thruster showed a very linear thrust to power relationship, as seen in Fig. 12, rather than the normal second order exponential shape. This is similar behaviour to other thrusters that have been directly compared a US and MS shielded configuration [21].

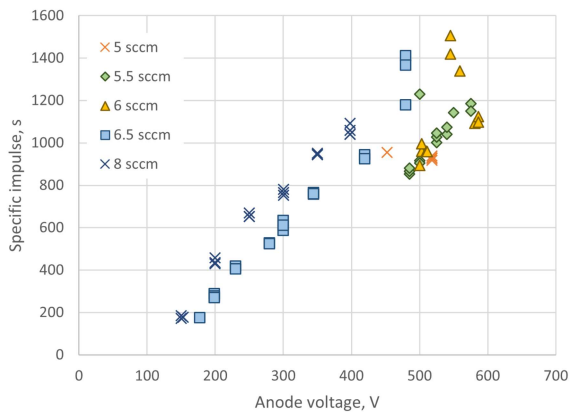

Figure 14: Effect of anode voltage on thruster specific impulse for various anode mass flow rates, all tests were operated in a voltage limited state.

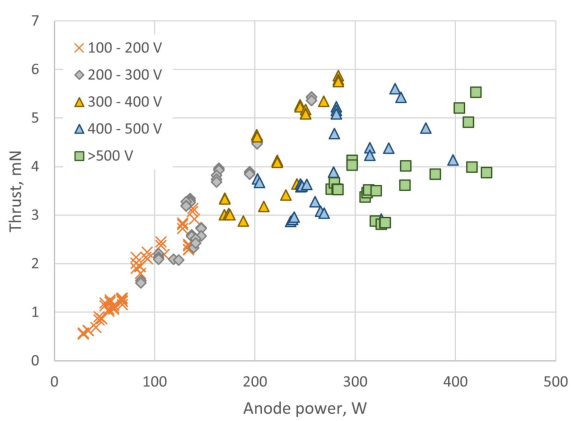

Figure 15: Thrust against power for different voltage ranges.

4.1.2 Voltage

Here the data collected from the thruster has been grouped into anode voltage ranges. In Fig. 15 a clear relationship between higher voltages and higher thrust can be seen. The interesting relationship appears between 400 - 500 V. This is likely a result of at the higher voltages low mass flow rates (¡ 6 sccm) were required to manage the power. At these flow rates operation became more unstable and the thermal effects due to the high voltages caused fluctuations in anode currents.

4.2 Comparison to other Krypton HET

The comparison between the MaSHEKT-100 and a large database of published HETs at the Univer-

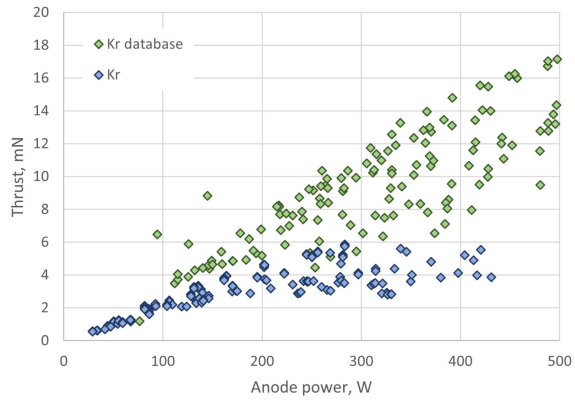

Figure 16: A comparison between the thrust against power for the MaSHEKT-100 and a large database of published HET performance data running on krypton [22, 23, 24, 25, 26, 27].

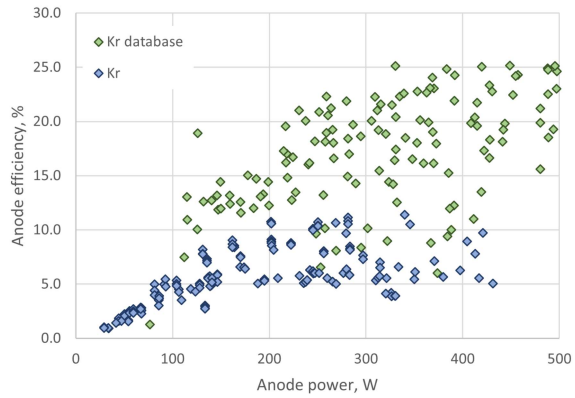

Figure 17: A comparison between the anode efficiency against power for the MaSHEKT-100 and a large database of published HET performance data running on krypton [22, 23, 24, 25, 26, 27].

sity of Southampton can be seen in Fig. 16 and 17. Here it can be seen that the thruster performance is of similar trend between 40 - 200 W, as this is the designed operational range, whilst failing to compete at higher powers which is to be expected [22, 23, 24, 25, 26, 27].

4.3 Evaluation of erosion

As can be seen in Fig 18, there is no obvious wear, but some pitting of the boron nitride channel was observed. It is unclear as the origin of the blackening of the channel, either from impurities in the additively manufactured anode or returned splutter from the graphite beam dump in the large vacuum chamber. The absence of the deposit at the exit could suggest either some level of erosion is present or that the mechanism of the deposition cannot exist at the conditions near the exit.

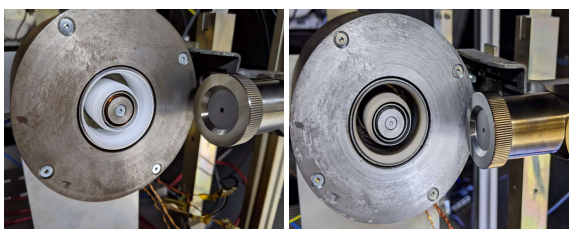

Figure 18: Pictures taken of the thruster before and after testing. The first image before any testing and the second was taken after approximately 30 - 45 hours of operation.

5. CONCLUSION & FUTURE WORK

In this paper the successful process from inception to initial testing of a low powered krypton Hall effect thruster with magnetic shielding has been presented and discussed. The process from start to end was under 1 year for design, manufacture and testing, whilst the cost of thruster itself was ¡£1000 for materials and manufacture. The thruster preformed as expected and was likely a design optimal for anode powers of $\approx 150 - 230\ W$. Thrust was measured using a pendulum thrust stand and anode efficiency and specific impulse was also calculated. The thruster operated well but could become unreliable at high anode voltages ($> 400\ V$) and low mass flow rate (< 5.5 sccm). The project has been successful in producing an operational low power krypton Hall effect thruster which will hopefully operate as a test bed for future testing of alternative propellants at the University of Southampton.

The design was intended to be a test platform for further investigation of alternative propellants at the University of Southampton, with work now continuing to operate this thruster on a range of gaseous propellants.

REFERENCES

[1] Käthe Dannenmayer and Stéphane Mazouffre. Elementary scaling relations for hall effect thrusters. *Journal of Propulsion and Power*, 27(1):236–245, 2011.

[2] Eunkwang Lee, Younho Kim, Hodong Lee, Holak Kim, Guentae Doh, Dongho Lee, and Wonho Choe. Scaling approach for sub-kilowatt hall-effect thrusters. *Journal of Propulsion and Power*, 35(6):1073–1079, 2019.

[3] Andrew Tisdall Peter, Edward Dyer, Charles Ryan, Vincent Garcia, and Alain Demaire. Initial investigation of alternative propellants for use with a low-power cylindrical hall thruster. In *Space Propulsion 2018*, May 2018.

[4] Stephan Zurbach, N Cornu, and P Lasgorceix. Performance evaluation of a 20 kw hall effect thruster. *Proc. IEPC 2011 (Kurhaus, Wiesbaden, Germany)*, 2011.

[5] Jonathan C McDowell. The low earth orbit satellite population and impacts of the spacex starlink constellation. *The Astrophysical Journal Letters*, 892(2):L36, 2020.

[6] Michel Moisan and Jacques Pelletier. *Physics of collisional plasmas: introduction to high-frequency discharges*. Springer Science & Business Media, 2012.

[7] Kybeom Kwon. *A novel numerical analysis of hall effect thruster and its application in simultaneous design of thruster and optimal low-thrust trajectory*. PhD thesis, Georgia Institute of Technology, 2010.

[8] R Rejoub, BG Lindsay, and RF Stebbings. Determination of the absolute partial and total cross sections for electron-impact ionization of the rare gases. *Physical Review A*, 65(4):042713, 2002.

[9] Philip L Bartlett and Andris T Stelbovics. Calculation of electron-impact total-ionization cross sections. *Physical Review A*, 66(1):012707, 2002.

[10] Robert C Wetzel, Frank A Baiocchi, Todd R Hayes, and Robert S Freund. Absolute cross sections for electron-impact ionization of the rare-gas atoms by the fast-neutral-beam method. *Physical Review A*, 35(2):559, 1987.

[11] Kathe Dannenmayer and Stephane Mazouffre. Sizing of hall effect thrusters with input power and thrust level: An empirical approach. *arXiv preprint arXiv:0810.3994*, 2008.

[12] Noah Zachary Warner. *Theoretical and experimental investigation of Hall thruster miniaturization*. PhD thesis, Massachusetts Institute of Technology, 2007.

[13] Dan M Goebel and Ira Katz. *Fundamentals of electric propulsion: ion and Hall thrusters*, volume 1. John Wiley & Sons, 2008.

[14] Yu Daren, Ding Yongjie, and Zeng Zhi. Improvement on the scaling theory of the stationary plasma thruster. *Journal of Propulsion and Power*, 21(1):139–143, 2005.

[15] George-Cristian Potrivitu. *Design and Computational Analysis of a Hall Effect Thruster Using a Novel Dimensioning Tool*. Bachelor's thesis, Military technical academy Bucharest, 07 2014.

[16] Michael J Sekerak. *Plasma Oscillations and Operational Modes in Hall Effect Thrusters*. PhD thesis, University of Michigan, 2014.

[17] Kybeom Kwon, Dimitri Mavris, and Mitchell Walker. New approach to numerical analysis of the hall thruster. In *46th AIAA/ASME/SAE/ASEE Joint Propulsion Conference & Exhibit*, page 6523, 07 2010.

[18] Kristi de Grys, Alex Mathers, Ben Welander, and Vadim Khayms. Demonstration of 10,400 hours of operation on 4.5 kw qualification model hall thruster. In *46th AIAA/ASME/SAE/ASEE Joint Propulsion Conference & Exhibit*, page 6698, 2010.

[19] Ryan Conversano. *Low-power magnetically shielded Hall thrusters*. PhD thesis, UCLA, 2015.

[20] Alberto Rossi, Frédéric Messine, and Carole Henaux. Parametric optimization of a hall effect thruster magnetic circuit. *Transactions of the Japan Society for Aeronautical and Space Sciences, Aerospace Technology Japan*, 14(ists30):Pb_197–Pb_202, 2016.

[21] Cosimo Ducci, Tommaso Misuri, Stefan Gregucci, Daniela Pedrini, and Kathe Dannenmayer. Magnetically shielded ht100 experimental campaign. *Proc. of the 35th IEPC*, 2017.

[22] Jesse A Linnell and Alec D Gallimore. Efficiency analysis of a hall thruster operating with krypton and xenon. *Journal of Propulsion and Power*, 22(6):1402–1418, 2006.

[23] Jesse Allen Linnell. *An evaluation of krypton propellant in Hall thrusters*. PhD thesis, University of Michigan, January 2007.

[24] David Jacobson and David Manzella. 50 kw class krypton hall thruster performance. In *39th AIAA/ASME/SAE/ASEE Joint Propulsion Conference and Exhibit*, page 4550, 2003.

[25] Michael R Nakles, William A Hargus Jr, Jorge J Delgado, and Ronald L Corey. A performance comparison of xenon and krypton propellant on an spt-100 hall thruster (preprint). Technical report, AIR FORCE RESEARCH LAB EDWARDS AFB CA, 2011.

[26] Thomas Malachi Andreano. *Performance and plume characterization of a laboratory krypton Hall thruster*. PhD thesis, Colorado State University, 2020.

[27] Jacek Kurzyna, Maciej Jakubczak, Agnieszka Szelecka, and Käthe Dannenmayer. Performance tests of ipplm's krypton hall thruster. *Laser and Particle Beams*, 36(1):105, 2018.